Check for updates

Original Research Article

Stage-specific cardiotoxicity induced by bisphenol A using human pluripotent stem cell-derived 2D- and 3D-cardiomyocyte models

Journal of Tissue Engineering
Volume 16: 1–16
© The Author(s) 2025
Article reuse guidelines:
sagepub.com/journals-permissions
DOI: 10.1177/20417314251383006
journals.sagepub.com/home/tej
Sage

Soon-Jung Park[1,2,*], Seong Woo Choi[3,*], Yun-Gwi Park[4,*], Hye-Eun Shim[5,6], Ji-hee Choi[4], Kang Moo Huh[6], Sung-Hwan Moon[4,#] and Sun-Woong Kang[5,7,#]

Abstract

Bisphenol A (BPA), a widely used industrial chemical with endocrine-disrupting properties, raises developmental and cardiotoxicity concerns. We established a stage-specific cardiotoxicity platform using human pluripotent stem cell (hPSC)-derived cardiomyocytes in two-dimensional and three-dimensional (3D) cultures. BPA exposure at ⩾10 μM significantly reduced cell viability and downregulated pluripotency and cardiac lineage markers such as OCT4, NKX2-5, and cTnT in a stage-dependent manner. Electrophysiological analysis revealed that acute exposure to 10 μM BPA disrupted action potentials in hPSC-derived cardiomyocytes, inducing membrane depolarization and rhythm disturbances. Furthermore, 3D cardiac tissues treated with 10 or 50 μM BPA exhibited severe mitochondrial deformation and impaired contractile function, as observed by TEM and beating analysis. Reproducing these effects in a personalized hPSC line validated the platform's applicability for patient-specific toxicity assessment. These findings highlight the importance of integrating developmental stage-specific and 3D human-relevant models for comprehensive cardiotoxicity evaluation of environmental chemicals such as BPA.

Keywords

bisphenol A, cardiotoxicity, human pluripotent stem cell-derived cardiomyocyte, alternative toxicity testing, 3D cell culture

Received: 19 April 2025; accepted: 13 September 2025

[1]R&D Center, Biosolvix Co. Ltd, Seoul, Republic of Korea
[2]Department of Medicine, Konkuk University School of Medicine, Seoul, Republic of Korea
[3]Department of Physiology, Dongguk University College of Medicine, Gyeongju-si, Gyeongsangbuk-do, Republic of Korea
[4]Department of Animal Science and Technology, Chung-Ang University, Anseong-si, Gyeonggi-do, Republic of Korea
[5]Center for Biomimetic Research, Korea Institute of Toxicology, Daejeon, Republic of Korea
[6]Department of Polymer Science and Engineering, Chungnam National University, Daejeon, Republic of Korea
[7]School of Korea Institute of Toxicology, University of Science and Technology, Daejeon, Republic of Korea

*These authors are co-first authors and contributed equally to this work.

#These authors contributed equally as corresponding authors.

Corresponding authors:
Sung-Hwan Moon, Department of Animal Science and Technology, Chung-Ang University, 4726, Seodong-daero, Daedeok-myeon, Anseong-si, Gyeonggi-do 17546, Republic of Korea.
Email: moonsh@cau.ac.kr

Sun-Woong Kang, Center for Biomimetic Research, Korea Institute of Toxicology, 141, Gajeong-ro, Yuseong-gu, Daejeon 34114, Republic of Korea.
Email: swkang@kitox.re.kr

Creative Commons Non Commercial CC BY-NC: This article is distributed under the terms of the Creative Commons Attribution-NonCommercial 4.0 License (https://creativecommons.org/licenses/by-nc/4.0/) which permits non-commercial use, reproduction and distribution of the work without further permission provided the original work is attributed as specified on the SAGE and Open Access pages (https://us.sagepub.com/en-us/nam/open-access-at-sage).

Introduction

Bisphenol A (BPA) is a widely used industrial chemical, commonly found in consumer products such as plastics, food packaging, and thermal paper.[1] Due to its extensive use in everyday materials, human exposure to BPA is universal, raising significant public health concerns.[2–4] BPA is well-known for its role as an endocrine disruptor, capable of interfering with hormonal signaling pathways.[1,5] Beyond its endocrine-disrupting effects, emerging research has highlighted BPA's broader capacity to induce cellular toxicity by disrupting fundamental biological processes, including cellular redox balance, mitochondrial function, and tissue-specific development.[6–8] These toxicological effects are of particular concern during early development, where precise cellular regulation is critical for proper organogenesis.[9,10]

Human pluripotent stem cells (hPSCs) serve as a powerful and human-relevant *in vitro* model for investigating the toxicological effects of chemicals such as BPA.[7,11] The hPSCs are capable of self-renewal and differentiation into various cell types, including cardiomyocytes, enabling the study of toxicities specific to critical stages of development.[12] By modeling different stages of differentiation—from undifferentiated hPSCs to cardiomyocyte induction and mature cardiomyocytes—it is possible to gain insights into the developmental windows of vulnerability where BPA exposure may be most harmful. This approach offers the advantage of mimicking human-specific biological processes that are difficult to replicate in animal models, which often exhibit species-specific responses to toxicants.

Moreover, the development of three-dimensional (3D) cell culture systems represents a significant advancement in the field of *in vitro* toxicology.[13,14] While traditional two-dimensional (2D) cultures are widely used, they do not fully capture the complex cellular architecture and microenvironment of living tissues.[15,16] In contrast, 3D cardiac tissue models recapitulate certain aspects of *in vivo* architecture, such as cell alignment and tissue compaction, and may therefore provide a more relevant platform for assessing compound-induced functional changes than conventional 2D cultures,[17,18] allowing for the investigation of organ-level responses to toxicants.[19,20] Importantly, recent studies have demonstrated that 3D cultures are superior in revealing subtle toxicological effects that may go unnoticed in 2D systems, such as changes in mitochondrial morphology and electrophysiological function.[21] Accordingly, research on the development of 3D cell models for drug toxicity assessment is actively being conducted. Notably, studies have focused on 3D-printed hepatocyte models for evaluating acetaminophen-induced hepatotoxicity,[22] as well as cell models that mimic epithelial tissues of the lung[23,24] or intestine.[25,26] Additionally, these 3D cell models are expected to provide valuable insights into the impact of xenobiotics such as BPA on cardiac tissues.[27,28]

In this study, we established an *in vitro* cyto- and cardio-toxicity evaluation platform based on a stage-specific model representing the entire process of cardiac development using a cardiomyocyte-specific reporter PSC line. To evaluate the potential applicability of this platform as a personalized toxicity evaluation system, we assessed and compared the toxic effects of BPA on another PSC line. Furthermore, to overcome the physiological limitations of conventional 2D models, we developed a 3D cardiac model using tissue engineering techniques after the cardiomyocyte differentiation stage. Through structural and functional analyses of mitochondria, we aimed to establish a cardiotoxicity assessment system that integrates 3D models with improved physiological relevance (Figure 1).

We propose a novel platform for developmental stage-specific cardiotoxicity assessment, integrating a reporter-based cell line, personalized hPSC applications, and 3D tissue engineering techniques. This multi-layered approach provides a comprehensive strategy for evaluating cardiotoxicity and can be utilized in various fields, including cardiotoxicity research, personalized medicine, and drug safety assessment.

Materials and methods

Chemicals

Matrigel hESC-qualified matrix was supplied by Corning (Corning, NY, USA). StemMACS™ iPS-Brew XF was purchased from Miltenyi Biotec (Bergisch Gladbach, Germany). UltraPure™ 0.5 M EDTA, RPMI1640, B-27™ Supplement (minus insulin), Advanced Minimum Essential medium (Advanced MEM), Dulbecco's Phosphate Buffered Saline (DPBS), GlutaMAX Supplement, TRIzol™ Reagent, Vitronectin, TRA-1-60, and Lipofectamine RNAiMAX were purchased from ThermoFisher Scientific (Waltham, MA, USA). Y-27632 and CHIR99021 were supplied by Tocris (Bristol, UK). Wnt-C59 was purchased from Selleck Chem (Houston, TX, USA). The High-Capacity cDNA Reverse Transcription Kit was purchased from Applied Biosystems (Waltham, MA, USA). FastStart Essential DNA Green Master was supplied from Roche (Basel, Switzerland). Normal goat serum, Anti-Cardiac Troponin T antibody, and DAPI Staining Solution were purchased from Abcam (Cambridge, UK). Alexa Fluor® 647 Mouse Anti-Cardiac Troponin T was purchased from BD Biosciences (Franklin Lakes, NJ, USA). Cell Counting Kit-8 (CCK8) reagent was purchased from Dojindo Molecular Technologies (Kumamoto, Japan). All other chemicals including BPA were purchased from Sigma-Aldrich (St. Louis, MO, USA). BPA was dissolved in ethanol to prepare a 50 mM stock solution, which was

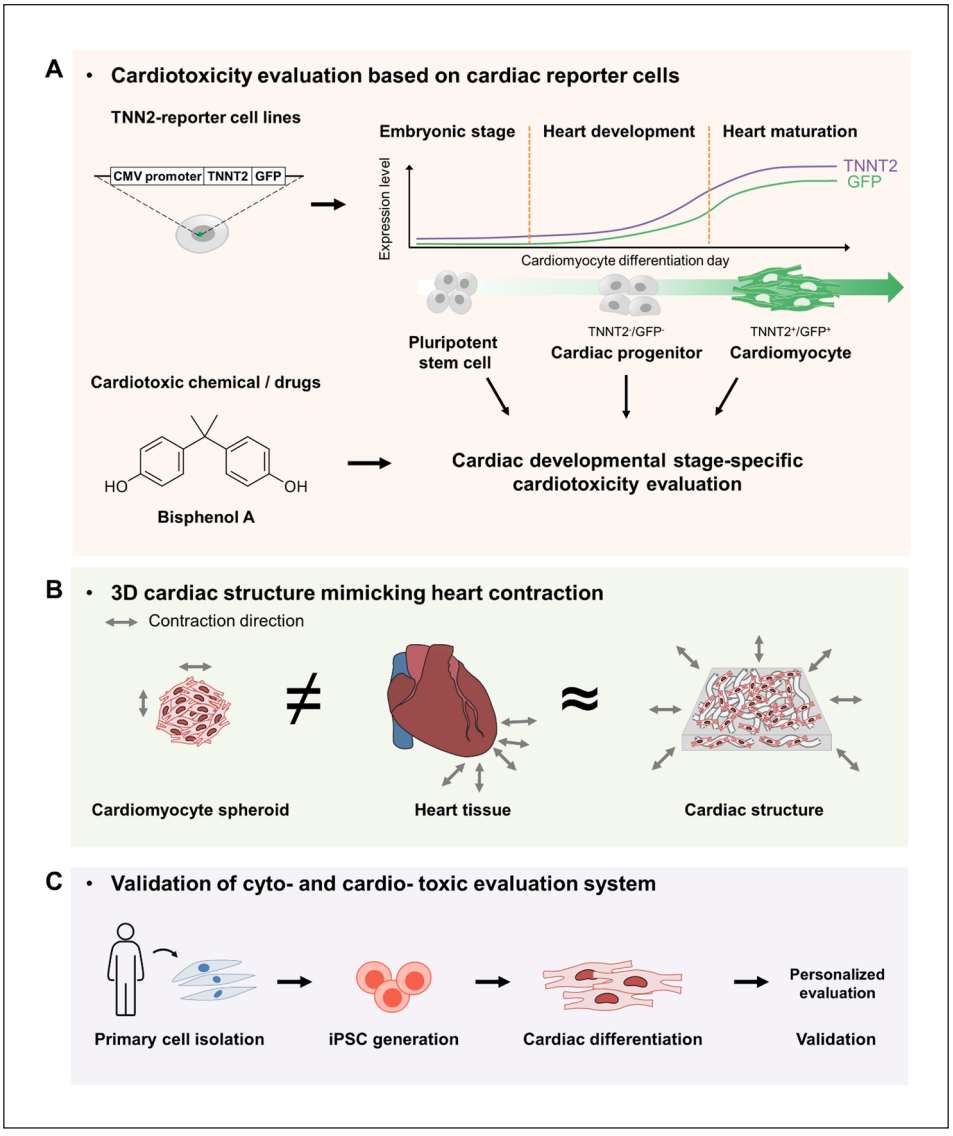


Figure. 1. Schematic diagram of experiments. (A) Cardiomyocyte specific reporter cell line, H9-hTnnT2-pGZ-TD2. The cell expresses GFP only when the cell line has been differentiated into a cardiomyocyte. The stage-specific cardiotoxicity evaluation platform was established based on BPA treatment. (B) Construction of collagen-based 3D cardiac structure mimicking heart contraction. (C) Validation of the platform for personalized applications.

subsequently diluted in culture medium to achieve final concentrations of 1, 10, 20, 50, and 100 µM.

Generation and maintenance of hPSCs

The cardiomyocyte-specific reporter cell line, H9-hTnnT2-pGZ-TD2, was purchased from WiCell (Madison, Wim USA). These cells do not exhibit GFP fluorescence in the undifferentiated state, but after cardiomyocyte differentiation, they display GFP fluorescence along with troponin T expression (Figure 1A). To generate a new human induced pluripotent stem cell line, ACE-hiPS-2, dermal fibroblasts from a 4-year-old male donor were reprogrammed using the StemRNA™ 3rd Gen Reprogramming Kit (Reprocell, Yokohama, JP) following the manufacturer's protocol. Briefly, fibroblasts were plated on a vitronectin-coated 6-well plate at 2×10^5 cells/well on day 0. Daily transfections with the non-modified-RNA reprogramming cocktail were carried out from days 1 to 4 using Lipofectamine RNAiMAX. On days 10–12, iPSC colonies were identified by staining with the TRA-1-60 antibody. The TRA-1-60-positive colonies were isolated and re-plated on a vitronectin-coated dish. To maintain both hPSC lines in an undifferentiated state, the media were changed daily with StemMACS iPS-Brew XF and the cells were passaged onto vitronectin-coated dishes every 3-4 days using 0.5 mM Ultra-Pure™ EDTA, pH 8.0. After passage, the cells were incubated with 10 µM Y-27632 for 24 h.

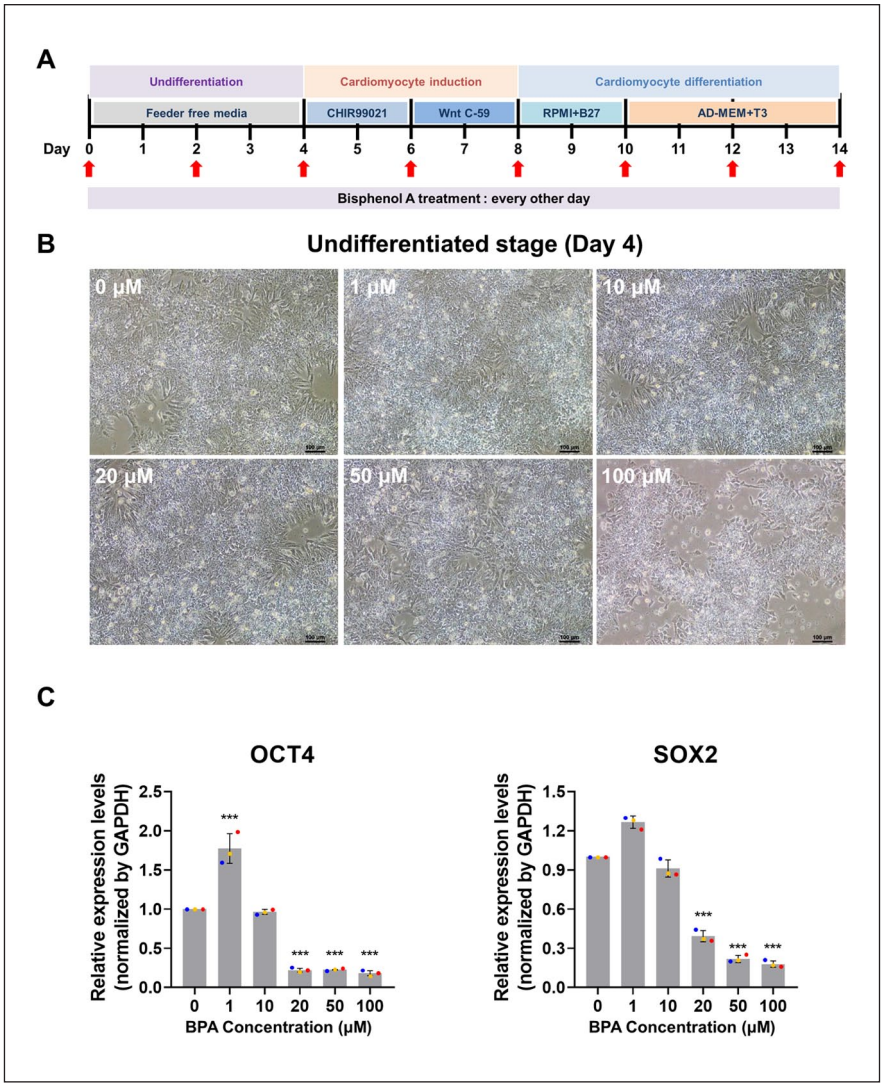


Figure 2. Analysis of the effects of BPA on hPSC culture stages. (A) Schematic strategy for BPA toxicity assessment at each stage of cardiomyocyte differentiation status. (B) Morphological changes observed in hPSCs treated with various concentrations of BPA during the undifferentiated stage. (C) Expression levels of pluripotency-related genes in hPSCs treated with various concentrations of BPA during the undifferentiated stage. Data represent mean ± standard deviation (SD) from three independent experimental batches. Colored dots indicate individual biological replicates. ***$p < 0.0001$ compared with 0 μM BPA treated group.

Differentiation of cardiomyocytes derived from hPSCs

Two hPSC lines, H9-hTnnT2-pGZ-TD2 from WiCell and ACE-hiPS2, were grown on Matrigel-coated dishes until they reached 90% confluency. To initiate differentiation into the cardiac lineage, the hPSCs were treated with 6 μM CHIR99021 in RPMI1640 medium supplemented with B-27™ Supplement (minus insulin). After 48 h, the medium was replaced with RPMI1640 medium containing 3 μM Wnt-C59 and B-27™ Supplement (minus insulin). For the specification stage, the medium was changed to Advanced MEM containing 2 mM GlutaMAX Supplement every 2 days starting from day 5. Contracting cells began to appear between day 6 and day 10. When contracting cardiomyocytes were observed, the medium was replaced every 2 days with Advanced MEM containing 100 ng/mL 3,3′,5-Triiodo-L-thyronine and 2 mM GlutaMAX Supplement.

BPA treatment

For BPA treatment in cell culture, the undifferentiated stage was treated for 4 days, the induction stage for 4 days, and the specification stage for 2 days (Figure 2A). Cells at each stage were treated with 1, 10, 20, 50, and 100 μM BPA. After adding BPA to the culture media, the media were replaced once every other day. For patch clamp analysis, BPA treatment was applied to contracting cardiomyocytes. After treatment, we washed out the cells with DPBS and confirmed the membrane potential.

Three-dimensional cell culture of hPSC-derived cardiomyocyte (hPSC-CMs) and analysis

To model the 3D cardiac structure, we prepared 3D cultures of cardiomyocytes using collagen matrices as a scaffold. The porous collagen matrix provided a large surface area for cell attachment and growth and facilitated the formation of new cardiac tissues (Figure 1B). Briefly, collagen matrices were prepared by cutting them into dimensions of $5 \times 5 \times 2\,mm^3$. Day 14 hiPSC-CMs differentiated without BPA exposure were harvested and diluted to a concentration of 4×10^6 cells/ml. A total of 50 µl of the cell suspension was gently added to each collagen matrix for absorption. Every hour, an additional 50 µl of culture medium was added three times to ensure sufficient cell attachment and absorption. Once the cells were adequately adhered, the cell-seeded collagen scaffolds were transferred to Ultra-Low Attachment culture dishes and incubated in Advanced MEM for 7 days. After 7 days of *in vitro* culture, BPA solutions (1, 10, and 50 µM in MEM) were added to the dishes containing the cell-seeded scaffolds and the medium was changed every 2 days (Figure 5A). After 14 days of 3D culture, we analyzed the scaffolds using transmission electron microscopy (TEM). For TEM analysis, we fixed the specimens in 2.5% (v/v) glutaraldehyde for 24 h, followed by dehydration with a series of graded ethanol and drying. The dried samples were mounted on a mixture of propylene oxide and Epon 812 media. The mounted samples were then cut into 70-nm-thick sections at a rate of 0.6 mm/s using an Ultra-Microtome (ULTRACUT UCT, LEICA, Wetzlar, GE) and placed on a grid for observation. Samples were imaged using TEM (JEM-1400Plus and JEM-1000BEF, JEOL, Tokyo, Japan) at 120 kV and 1000 kV.

To evaluate mitochondrial morphology under different BPA concentrations, TEM images were analyzed using ImageJ software (NIH, Bethesda, MD, USA), as previously described.[29] For each sample, a minimum of five randomly selected fields were analyzed, and at least 20 mitochondria were evaluated per group. Mitochondrial parameters, including area (μm^2) and circularity, aspect, cristae score, were quantified by manually tracing the outer mitochondrial membrane using the freehand selection tool. Mitochondrial elongation was quantitatively assessed using two complementary shape descriptors: circularity index and aspect ratio. The circularity index, calculated as $4\pi \times \text{Area}/(\text{Perimeter})^2$, ranges from 0 to 1, with values closer to 1 indicating round mitochondria and lower values indicating more elongated or irregular shapes. The aspect ratio, defined as the ratio of the major to minor axis length, increases with mitochondrial elongation. Together, these two parameters provide a comprehensive measure of mitochondrial shape and elongation. In addition, the morphology of the cristae was semi-quantitatively assessed by assigning each mitochondrion a cristae score from 0 to 4, where 0 indicates no clearly defined cristae; 1, more than 50% of the mitochondrial area is lacking cristae; 2, more than 25% of the area is lacking cristae; 3, numerous cristae present in over 75% of the area but irregular in shape; and 4, numerous and well-organized, regular cristae.

Quantitative RT-PCR

Total RNA was extracted using the TRIzol reagent. RNA concentration was measured using a NanoDrop One C Microvolume UV-V Spectrophotometer and cDNA was synthesized with the High-Capacity cDNA Reverse Transcription Kit following the manufacturer's instructions. Real-time PCR was conducted using SYBR Green expression assays on a LightCycler® 96 Real-Time PCR System (Roche, Basel CH), and the samples were normalized to the GAPDH housekeeping gene. The gene expression level was calculated using the ΔΔCt method. The primer sequences are provided in Table S1.

Immunocytochemistry

Cells were fixed with 4% paraformaldehyde for 20 min and permeabilized with 0.1% Triton X-100 in PBS for 10 min. After treatment with 5% normal goat serum for 30 min, the cells were stained with cardiac troponin T (cTnT) and sarcomeric-α-actinin for 16 h at 4 °C. Cells were washed three times with PBS and then incubated with Alexa Fluor 488-or 594-conjugated secondary antibodies for 1 h. Nuclei were stained with DAPI. All images were analyzed using a fluorescence microscope.

Cell viability assay

Cell viability was detected using a CCK-8 assay. ACE-hiPS2 cells were seeded at a density of 5×10^4/a well of 24-well plates with 1, 10, and 50 µM BPA, followed by the addition of 10 µl CCK8 reagent (Dojindo Molecular Technologies) to each well and incubation at 37°C for 30 min. Then the absorbance at 450 nm was measured using a Cytation C10 (BioTek, Winooski, VT, USA).

Flow cytometry (FC) analysis

The hPSC-CMs were collected and washed with FACS solution (PBS supplement 2% FBS). The single cells were incubated with Alexa Fluor 647-conjugated anti-cTnT for 30 min at 4℃, followed by three washes in FC solution. FC analysis was performed using a SONY® flow cytometer SH800 (Sony Biotechnology, Inc., Tokyo, Japan) with Sony software version 2.1.5.

Electrophysiological recording and analysis

A conventional whole-cell patch clamp was used to record the action potential in hPSC-CMs. A spontaneously beating cardiomyocyte was selected for current-clamp action

potential recording using an Axopatch 200B amplifier (Axon Instruments, Foster, CA, USA) and a Digidata 1440B AD-DA converter (Axon Instruments). The action potential parameters, including APD90c (action potential duration at 90% repolarization with Fridericia's rate correction), APA (action potential amplitude), V_{max} (maximum upstroke velocity), and beat period, were analyzed using the Clampfit 11 program (Axon Instruments, Molecular Devices, San Jose, CA, USA). The extracellular solution used for recording the action potential contained 145 mM NaCl, 5.4 mM KCl, 10 mM HEPES, 1 mM $MgCl_2$, 1.8 mM $CaCl_2$, and 5 mM glucose adjusted to pH 7.4 with NaOH. The intracellular solution contained 120 mM K-aspartate, 20 mM KCl, 5 mM NaCl, 2 mM $CaCl_2$, 5 mM EGTA, 10 mM HEPES, and 5 mM Mg-ATP adjusted to pH 7.25 with KOH.

Statistical analysis

All experiments were performed in at least three independent experimental batches, and data are presented as mean ± standard deviation (SD). Statistical comparisons between two groups were performed using two-tailed Student's *t*-tests. For comparisons among three or more groups, one-way ANOVA followed by Tukey's post hoc test was used. All statistical analyses and data visualization were performed using GraphPad Prism version 5 (GraphPad Software, San Diego, CA, USA). The statistically significant differences are indicated by $*p < 0.05$, $**p < 0.005$, or $***p < 0.0001$.

Results

Reporter cell-line-based system for cytotoxicity evaluation during cardiomyocyte development

To establish a platform to evaluate cytotoxicity at various stages of cardiomyocyte differentiation and development, we used the H9-hTnnT2-pGZ-TD2 embryonic stem cell line, which expresses a fluorescent reporter for the cardiomyocyte-specific marker troponin T.[30] Cardiomyocyte differentiation was conducted in three stages: a 4-day undifferentiation stage, a 4-day cardiomyocyte induction stage, and a 6-day cardiomyocyte differentiation stage following a previously described protocol.[28,31–33] In addition, cardiomyocytes differentiated in culture dishes were cultured in a 3D structure for 7 days after differentiation to evaluate whether they could mimic the actual human heart. To evaluate the cardiotoxic effects at all stages of cardiomyocyte development, cardiomyocytes were treated with various concentrations of BPA, a representative endocrine disruptor, every other day to compare and analyze the morphological and molecular characteristics and functions of cardiomyocytes (Figure 2A).

To investigate the cytotoxic effect of BPA at the undifferentiated stage, we treated cells in culture at the undifferentiated stage with 1, 10, 20, 50, and 100 μM BPA for 4 days. No morphological changes were observed in the 1, 10, and 20 μM BPA treatment groups compared to the control group. However, cell density was significantly lower in the 100 μM BPA treatment group on day 4 (Figure 2B). To confirm the morphological toxicity of BPA at the molecular level, we examined the expression of pluripotency marker genes *OCT4* and *SOX2* using qRT-PCR. The expression of *OCT4* and *SOX2* increased in the 1 μM BPA treatment group and was similar to the control group in the 10 μM BPA treatment group. However, in the 20, 50, and 100 μM BPA treatment groups, the expression of undifferentiated gene markers was significantly reduced compared to the control group (Figure 2C). These findings established the cytotoxic evaluation system in the pluripotent stem cell maintenance stage and confirmed the cytotoxic effects of BPA at high concentrations.

To confirm the effect of BPA at the cardiac induction stage, we differentiated the BPA-treated cells to cardiac progenitors while continuing to treat them with the same concentration of BPA for an additional 4 days (Figure 3). There were no morphological changes in the 1 or 10 μM BPA treatment groups compared to the control group (Figure 3A). However, in the 100 μM BPA treatment group, noticeable cell detachment was observed. We then confirmed the expression of genes specific to the three germ layers in the BPA-treated cardiomyocyte induction stage using qRT-PCR. The expression of all genes was significantly reduced in the 50 and 100 μM BPA treatment groups. In detail, the endoderm-specific gene *AFP* was expressed at a similar level to the control group in the 1, 10, and 20 μM BPA treatment groups. *SMA*, a mesoderm-specific gene, showed higher expression in the 1 μM BPA treatment group compared to the control group and was expressed at a level similar to the control group in the 10 μM BPA treatment group. However, *SMA* expression significantly decreased in the 20 μM BPA treatment group. *TUJ1*, an ectoderm-specific gene, was expressed at a level similar to the control group in the 1 μM BPA treatment group, but its expression significantly decreased in the 10 and 20 μM BPA treatment groups. Through this, it was confirmed that treatment with BPA concentrations of 20 μM or higher in the cell model, which mimics the early heart development process, changed the morphological characteristics and viability of cells.

To investigate the cytotoxic effect of BPA at the cardiomyocyte differentiation stage, we differentiated the BPA-treated cells into cardiomyocytes while continuing to treat them with the same concentration of BPA (Figure 4). We observed whole-cell detachment in the 20, 50, and 100 μM BPA treatment groups. The cells survived only in the 0, 1, and 10 μM BPA treatment groups and spontaneous beating cardiomyocytes were observed on day 14 in these groups. The beating cardiomyocytes expressed green fluorescence (Figure 4A). These cells did not exhibit spontaneous beating nor express GFP fluorescence. We then

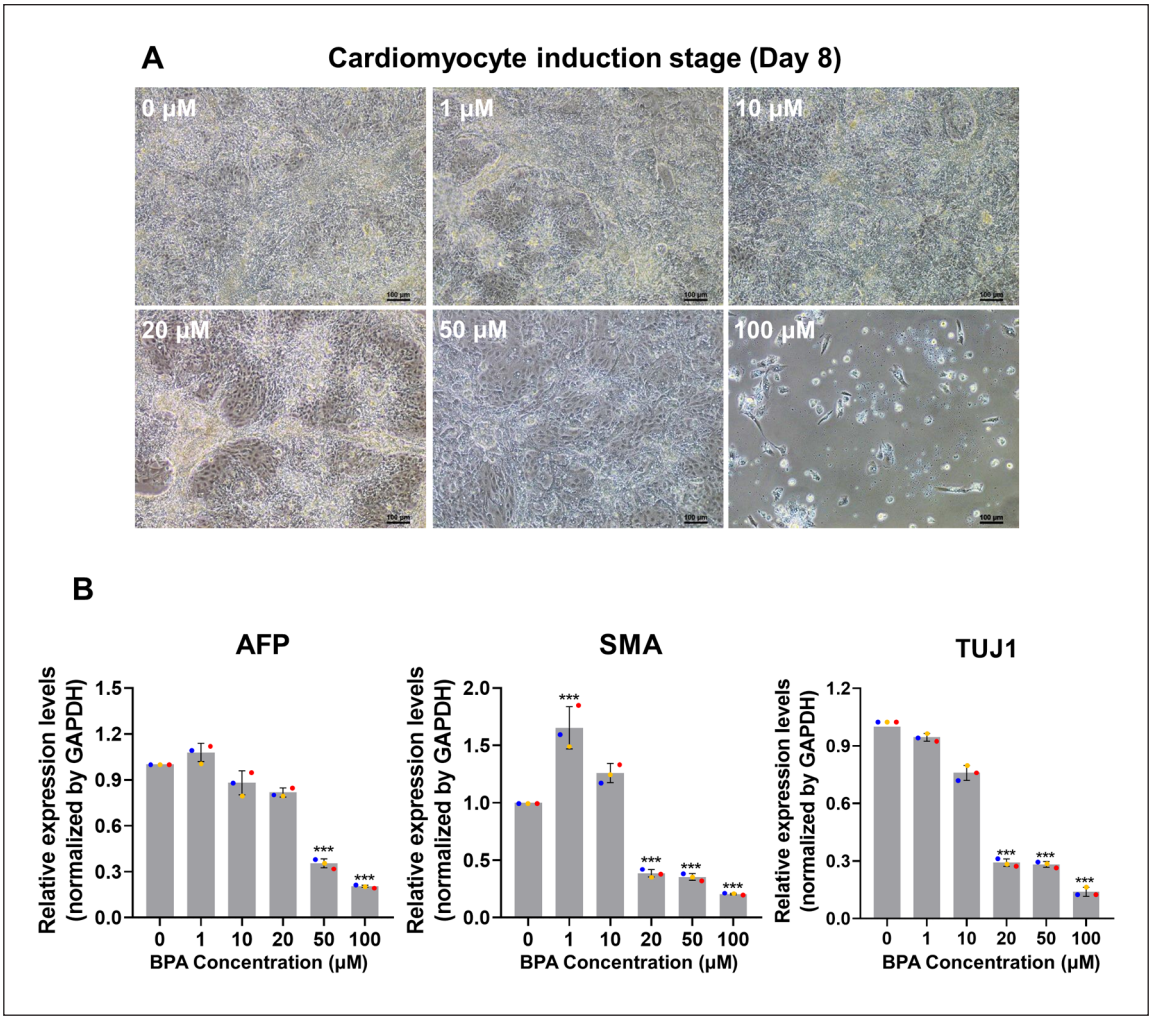


Figure 3. Analysis of the effects of BPA on the hPSC-derived cardiomyocyte induction stage. (A) Observation of morphological changes following treatment with various concentrations of BPA in the cardiomyocyte induction stage. (B) Expression of representative genes from the three germ layers in hPSC derivatives following treatment with various concentrations of BPA in the cardiomyocyte induction stage. Data represent mean ± standard deviation (SD) from three independent differentiation batches. Colored dots indicate individual biological replicates. ***$p < 0.0001$ compared with 0 μM BPA treated group.

investigated the expression of genes specific to the three germ layers in the BPA-treated cardiomyocyte induction stage using qRT-PCR (Figure 4B). The pluripotency marker gene *OCT4* was significantly down-regulated, while the cardiomyocyte-specific genes *NKX2.5* and *cTnT* were up-regulated in the 0 and 1 μM BPA treatment groups compared to the negative control group (undifferentiated stage). In contrast, the 10 μM BPA treatment group showed decreased gene expression compared to both the 0 μM BPA treatment group and similar with the negative control group (Figure 4B).

Evaluation of the electrophysiological function of cardiomyocytes in response to BPA treatment

To accurately investigate the effects of BPA exposure on actual cardiac function, we used patch clamp analysis to evaluate cardiac action potential properties (Figure 5) such as APA, V_{max}, beat period, and APD90c. We found that low-dose BPA treatments did not alter the cardiac action potential of hPSC-CMs (Figure 5A), and APA, Vmax, beat period, and APD90c analyses also showed no significant difference among the BPA treatment groups (Figure 5B). However, acute treatment with 10 μM BPA disrupted the spontaneously beating action potential (Figure 5C). In some cases, 10 μM BPA caused mild membrane potential depolarization, resulting in irregular action potential overshoots and beatings. The irregular action potential was restored to normal after washing out the BPA (Figure 5D). In conclusion, unlike high-dose BPA exposure, low-dose BPA exposure may improve heart function during development. However, exposure to >10 μM BPA may inhibit early cardiac occurrence, and acute treatment with 10 μM BPA may cause rhythmic disorder in hPSC-CMs due to membrane depolarization.

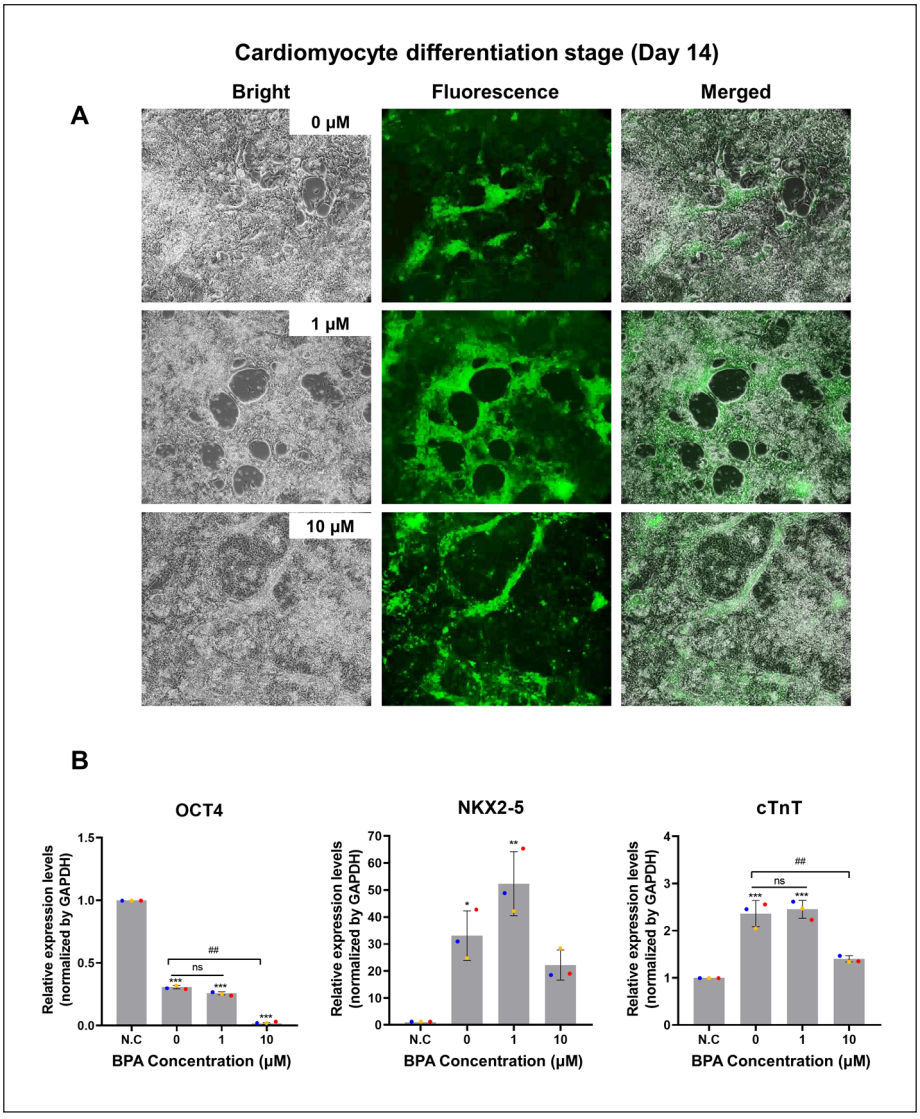


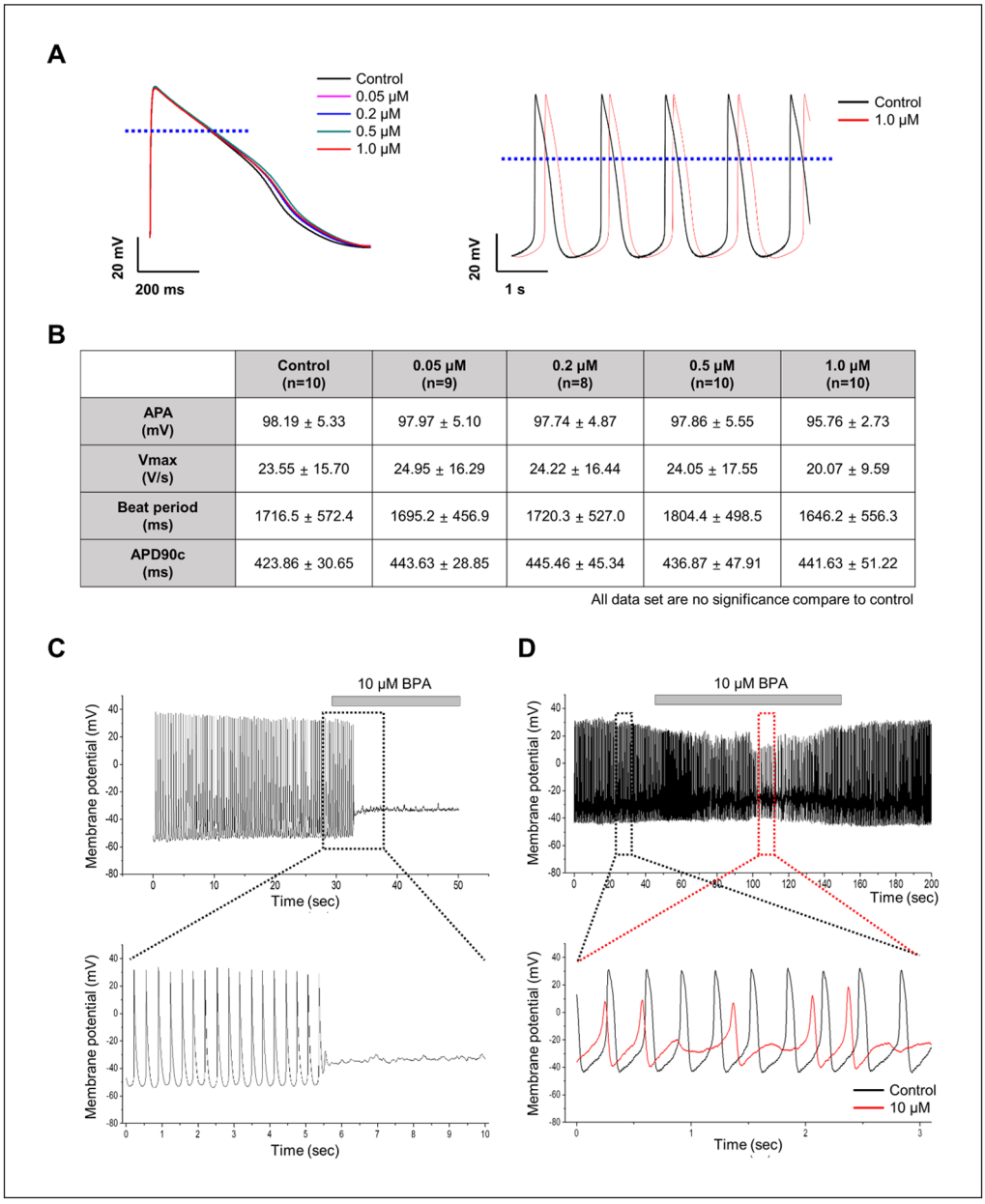
Figure 4. Analysis of the effects of BPA on the hPSC-derived cardiomyocyte differentiation stage. (A) Observation of cardiomyocyte differentiation with different BPA treatments in the cardiomyocyte differentiation stage. (B) Expression of pluripotency and cardiomyocyte-specific genes in hPSC-derived cardiomyocytes according to BPA treatments in the cardiomyocyte differentiation stage. Data represent mean ± standard deviation (SD) from three independent differentiation batches. Colored dots indicate individual biological replicates. $^{*}p < 0.05$, $^{**}p < 0.005$, $^{***}p < 0.0001$ compared with N.C group and $^{\#\#}p < 0.005$, $^{\#\#\#}p < 0.0001$ compared with 0 μM BPA treated group. N.C: Negative control (undifferentiated state).

These results are supported by a previous study demonstrating the toxic effects of BPA on rat embryonic cardiomyocyte differentiation and hPSC-CMs.[34]

Development of a toxicity test that uses a 3D cultured construct to mimic heart tissue

To analyze the functional and structural effects of BPA, we developed a 3D cardiac tissue model by mixing hPSC-derived cardiomyocytes with a collagen matrix (Figure 6A). After incubation, the hPSC-derived cardiomyocytes were organized with the collagen matrix, resulting in a porous structure. To examine the functional changes caused by BPA exposure at 1 μM and 10 μM, the effects of which cardiomyocytes were identified in the previous results, we conducted a structural analysis of the beating capabilities and mitochondria in the cardiac tissue (Figure 6B, Video S1-S4). The beating capabilities of the cardiac tissue were similar in the 1 μM and 10 μM BPA groups compared to the control. Notably, when the cardiac tissue was treated with 50 μM BPA, the beating rate was decreased (Video S4).

We examined the effects of BPA on mitochondria in 3D cardiac tissues using TEM (Figure 6C). In the control and 1 μM BPA groups, mitochondria appeared intact with well-defined cristae. However, in the 10 μM and 50 μM BPA



	Control (n=10)	0.05 μM (n=9)	0.2 μM (n=8)	0.5 μM (n=10)	1.0 μM (n=10)
APA (mV)	98.19 ± 5.33	97.97 ± 5.10	97.74 ± 4.87	97.86 ± 5.55	95.76 ± 2.73
Vmax (V/s)	23.55 ± 15.70	24.95 ± 16.29	24.22 ± 16.44	24.05 ± 17.55	20.07 ± 9.59
Beat period (ms)	1716.5 ± 572.4	1695.2 ± 456.9	1720.3 ± 527.0	1804.4 ± 498.5	1646.2 ± 556.3
APD90c (ms)	423.86 ± 30.65	443.63 ± 28.85	445.46 ± 45.34	436.87 ± 47.91	441.63 ± 51.22

All data set are no significance compare to control

Figure 5. Electrophysiological analysis of BPA-treated hPSC-derived cardiomyocytes. (A and B) Comparative analysis of the cardiac action potentials in hPSC-derived cardiomyocytes at various BPA concentrations. (C and D) Disruption of action potentials by acute treatment with 10 μM BPA in hPSC-derived cardiomyocytes.

groups, clear signs of mitochondrial damage were observed, such as swelling, rounded shape, and disrupted internal structure (yellow arrowheads). Quantitative analysis showed that mitochondria became more circular and less elongated at these higher concentrations. This shift suggests a loss of healthy, tubular morphology. In addition, the inner membrane structures, including cristae, were noticeably disorganized or diminished in the damaged mitochondria, indicating structural and possibly functional impairment. Mitochondrial deformation can affect the function of the respiratory chain, lead to cell apoptosis and necrosis, and interact with other cellular organs through mitochondrial permeability transition pores. These results suggest that exposure to BPA, particularly at concentrations $>10\,\mu M$, can lead to serious diseases in the early stages of heart development.

Application of cardiotoxicity evaluation system based on drug exposure frequency

To evaluate the applicability of our cardiotoxicity assessment platform using a reporter cell line, we investigated the effects of varying BPA exposure conditions on H9-hTnnT2-pGZ-TD2 cells (Figure 7). To assess the

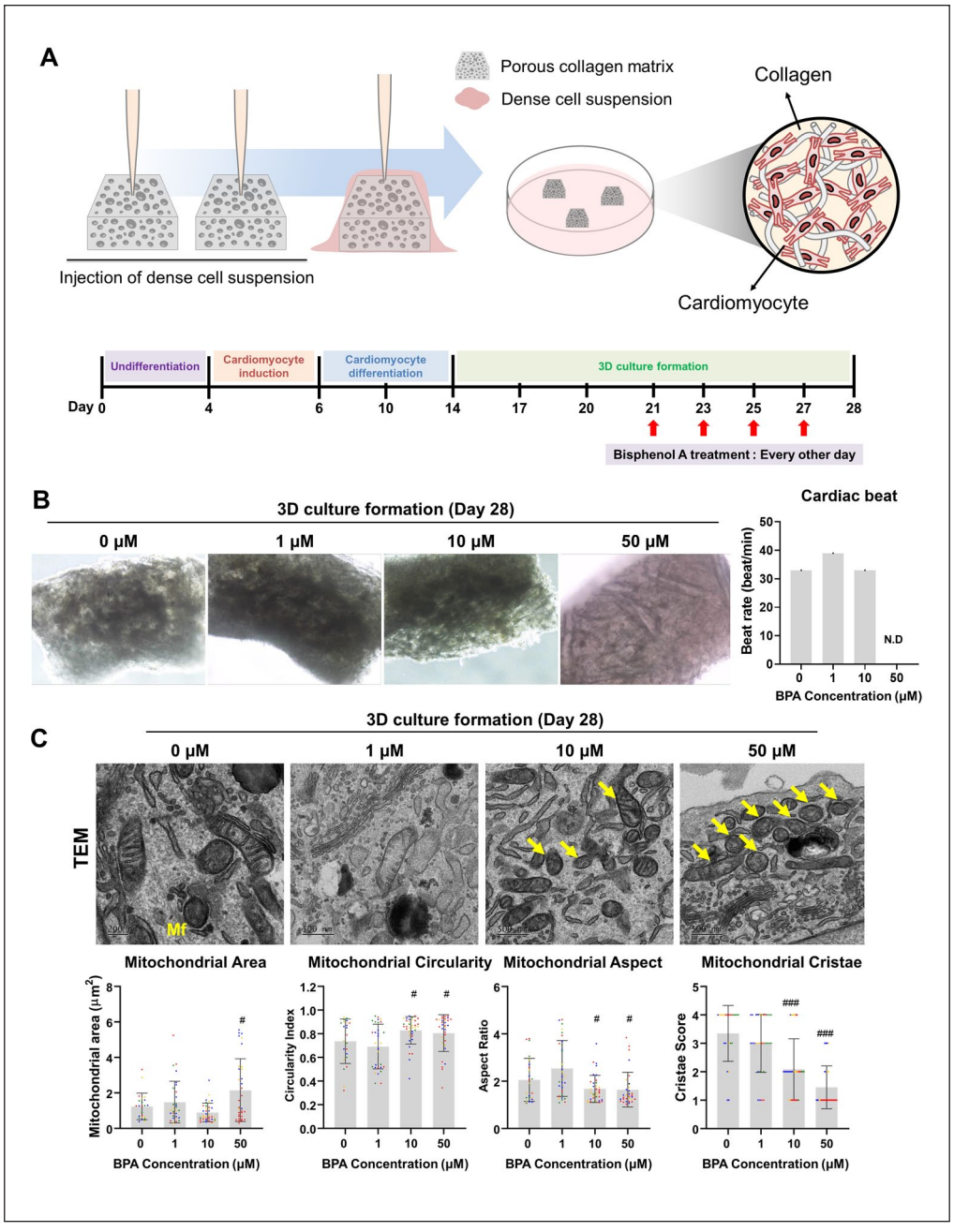


Figure 6. BPA toxicity test using a cardiac tissue 3D culture system. (A) Schematic strategy for generation of cardiac tissue with collagen matrix and cardiomyocytes. (B) Representative brightfield images of 3D cardiac tissues at day 28 with quantification of cardiac beating rates. (C) Representative TEM images of 3D-cultured cardiac tissues according to BPA treatment. Yellow arrows indicate abnormal mitochondria. Data represent mean ± standard deviation (SD) from at least three independent batches of differentiation and 3D cardiac tissues. Colored dots indicate individual biological replicates. $^{\#}p < 0.05$, $^{\#\#\#}p < 0.001$ compared with 0 μM BPA treated group.

impact of frequent BPA exposure during cardiac development, H9-hTnnT2-pGZ-TD2 cells were treated with BPA daily for 14 days, from the undifferentiated stage to the cardiomyocyte differentiation stage (Figure 7A). The differentiation efficiency was then evaluated by comparing the expression levels of troponin T. As a result, the 1 μM BPA-treated group exhibited fluorescence expression similar to that of the control group. However, in the 10 μM BPA-treated group, the number of fluorescence-expressing cells was significantly reduced compared to the control group (Figure 7B). These findings indicate that repeated exposure to BPA exerts greater toxicity on cardiac development. Furthermore, this result suggests that our cardiotoxicity assessment platform can evaluate drug toxicity across various concentrations and exposure durations.

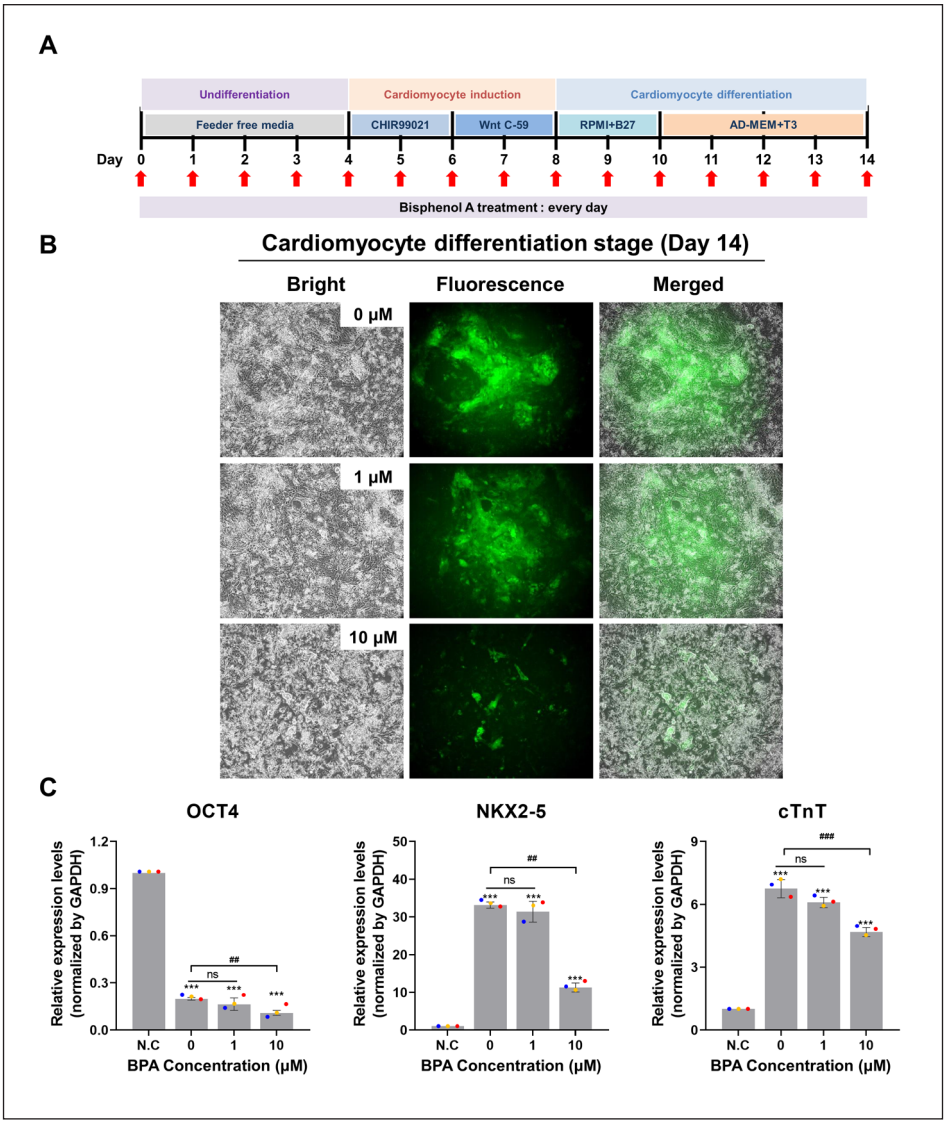


Figure 7. Evaluation of BPA-induced cardiotoxicity by exposure frequency. (A) Schematic of the strategy for BPA toxicity assessment under continuous BPA treatment. (B) BPA-induced cardiotoxicity evaluation by GFP expression. (C) Expression of pluripotency and cardiomyocyte-specific genes in hPSC-derived cardiomyocytes according to frequent exposure of BPA in the cardiomyocyte differentiation stage. Data represent mean ± standard deviation (SD) from three independent differentiation batches. Colored dots indicate individual biological replicates. $^{*}p < 0.05$, $^{**}p < 0.005$, $^{***}p < 0.0001$ compared with N.C group and $^{\#\#}p < 0.005$, $^{\#\#\#}p < 0.0001$ compared with 0 μM BPA treated group. $n = 3$. N.C: Negative control (undifferentiated state).

Application of the cytotoxic evaluation platform in personalized cell lines

To investigate whether the cardiotoxicity assessment platform established using a reporter cell line can be utilized as a personalized drug toxicity evaluation system (Figure 1C), we assessed functional changes following drug exposure in a newly generated pluripotent stem cell line, ACE-hiPS2 (Figure 8). We generated the ACE-hiPS2 stem cell line by reprogramming human dermal fibroblasts from a healthy individual (Figure S1). Subsequently, BPA was administered at various concentrations every other day from the undifferentiated stage to the cardiomyocyte differentiation stage, and the morphological, molecular, and functional characteristics of cardiomyocytes were analyzed. Similar to the results obtained using the reporter cell line, we observed a dose-dependent increase in toxicity with increasing BPA concentrations.

In the undifferentiated stage, no significant morphological changes were observed in the 1 and 10 μM BPA-treated groups compared to the control. However, in the 50 μM BPA-treated group, cell density was significantly reduced compared to the control group (Figure 8A). To quantitatively assess this, a cell viability assay was performed, revealing that while the 1 and 10 μM BPA-treated groups exhibited survival rates comparable to the control,

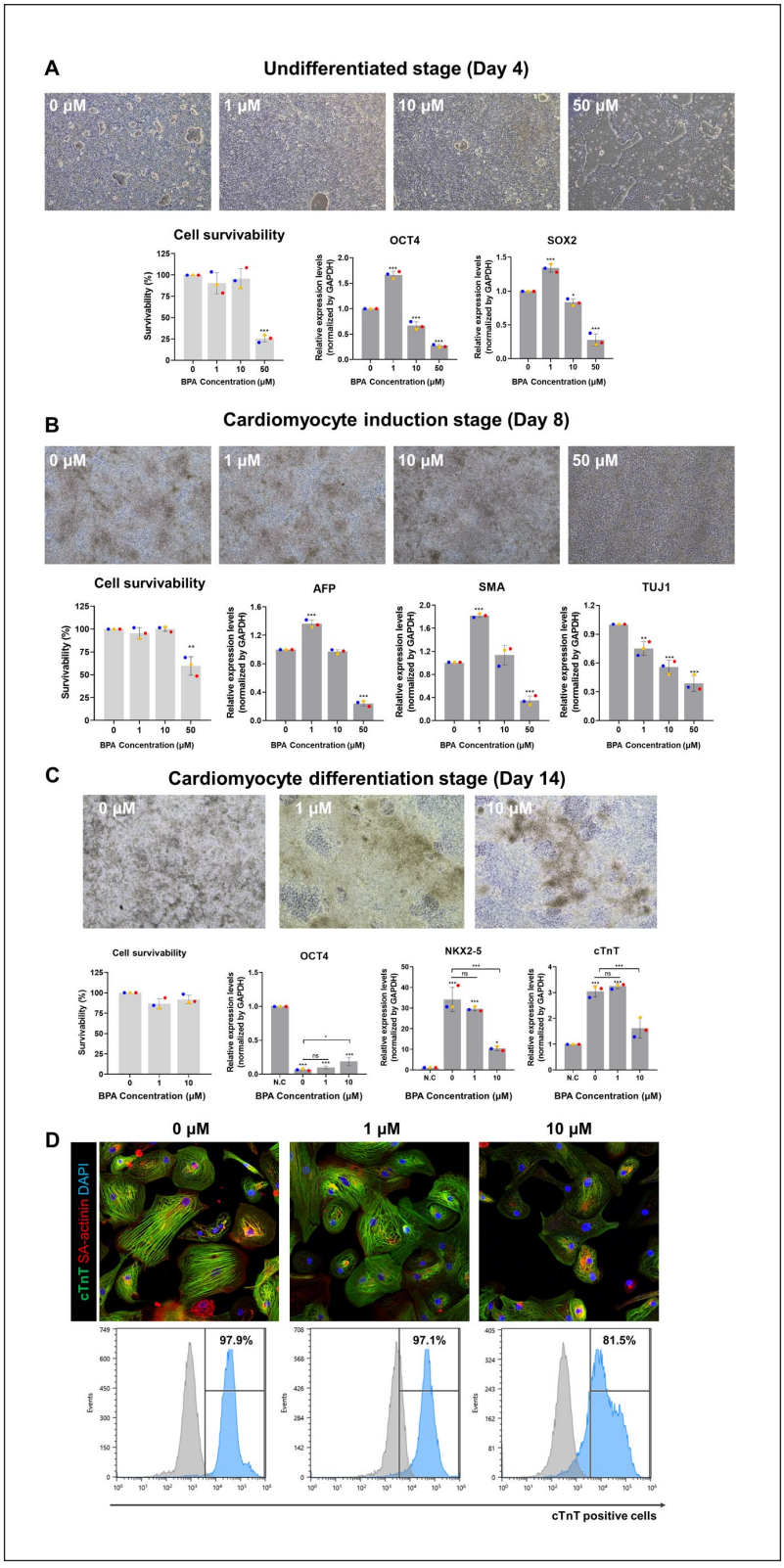


Figure 8. Evaluation of BPA-induced cardiotoxicity on personalized normal PSC cell lines. Analysis of the effects of BPA on hPSC culture (A), cardiac induction (B) and cardiomyocyte differentiation stage (C). Morphological observation, cell viability test, and gene expression were analyzed at each stage. Data represent mean ± standard deviation (SD) from three independent differentiation batches. Colored dots indicate individual biological replicates. *$p < 0.05$, **$p < 0.005$, ***$p < 0.0001$ compared with N.C or 0 μM BPA treated groups. (D) Immunostaining and flow cytometry analysis of BPA treated cardiomyocytes. N.C: Negative control.

the 50 μM BPA-treated group showed a significant reduction in viability. Consistent with previous findings in hTnnT2-pGZ-TD2 cells, these results indicate that high-concentration BPA exposure during the undifferentiated stage impairs the survival and proliferation of hPSCs. Additionally, qRT-PCR analysis of pluripotency marker genes (*OCT4* and *SOX2*) revealed that the 1 μM BPA-treated group exhibited higher gene expression levels than the control group, whereas the 10 and 50 μM BPA-treated groups showed reduced expression. Increased expression of pluripotency markers in the 1 μM BPA-treated group was also observed in hTnnT2-pGZ-TD2 cells, aligning with previous studies indicating that acute BPA exposure enhances pluripotency marker expression in mouse embryonic stem cells (ESCs).[35] Furthermore, high BPA concentrations induced dose-dependent morphological and molecular damage in hPSCs, similar to that observed in hTnnT2-pGZ-TD2 cells.

In the cardiomyocyte induction stage, the 1 and 10 μM BPA-treated groups did not exhibit significant morphological changes compared to the control, whereas the 50 μM BPA-treated group showed distinct morphological abnormalities (Figure 8B). Similarly, cell viability assays demonstrated that the 1 and 10 μM BPA-treated groups exhibited survival rates comparable to the control, while the 50 μM BPA-treated group showed a significant decrease in viability. Subsequent qRT-PCR analysis of three germ layer-specific genes revealed that the endoderm-specific gene (*AFP*) and mesoderm-specific gene (*SMA*) were upregulated in the 1 μM BPA-treated group, while their expression levels were similar to the control in the 10 μM BPA-treated group. However, in the 50 μM BPA-treated group, expression levels of *AFP* and *SMA* were significantly reduced. Additionally, the ectoderm-specific gene (*TUJ1*) was downregulated in all BPA-treated groups compared to the control. These results align with findings in hTnnT2-pGZ-TD2 cells and support previous research suggesting that BPA exposure disrupts germ layer-related gene expression in mouse ESCs.[36]

In the cardiomyocyte differentiation stage, 1 and 10 μM BPA-treated groups exhibited similar morphological characteristics and cell viability to the control group. However, qRT-PCR analysis of cardiomyocyte-specific marker genes (cTnT and SA-actinin) revealed that while the 1 μM BPA-treated group exhibited gene expression levels comparable to the control, the 10 μM BPA-treated group showed a significant reduction in expression (Figure 8C). Immunocytochemistry (ICC) analysis further confirmed reduced protein expression in the 10 μM BPA-treated group, and flow cytometry analysis indicated a lower proportion of $cTnT^+$ cells in this group (Figure 8D).

Taken together, our findings suggest that low-dose BPA exposure does not induce cytotoxicity during the differentiation of hPSC-derived cardiomyocytes. However, high-dose or frequent BPA exposure can lead to significant cytotoxic effects. These results are consistent with previous studies investigating BPA-induced cardiotoxicity in mouse ESCs and hPSCs.[8,36] Furthermore, this study confirms that the reporter cell-based cardiotoxicity assessment system we established is a broadly applicable platform for evaluating cardiotoxicity across various cell lines.

Discussion

In this study, we investigated the developmental and cardiotoxic effects of BPA using a cardiomyocyte-specific reporter cell line derived from hPSCs. By tracing morphological and genetic expression changes from the undifferentiated stage to the cardiomyocyte differentiation stage, we monitored BPA-induced toxicity across key phases of heart development. Furthermore, we evaluated the physiological relevance of our model by incorporating electrophysiological analyses and a 3D culture system that closely mimics the human heart environment. The established toxicity assessment platform was further expanded by introducing modified drug treatment conditions and a novel personalized cell line to explore its applicability for individualized toxicity screening.

Morphological and functional analyses using the cardiomyocyte-specific reporter line demonstrated significant developmental and functional cardiotoxicity following exposure to BPA concentrations above 10 mM. These findings are consistent with previous studies and support the reliability and validity of our approach.[37,38] Interestingly, exposure to a lower concentration of BPA (1 mM) appeared to enhance cardiac development, suggesting that BPA, as an endocrine-disrupting chemical, may exert hormone-like effects during cardiogenesis. This phenomenon was consistently reproduced in a personalized cell line, indicating that the observed cardiotoxic responses are not limited to a single cell line. Gene expression patterns, morphological changes, and functional outcomes were comparable between the two cell lines, demonstrating the reproducibility of the results and highlighting the potential of this platform to be applied more broadly in toxicological assessment.

One of the major contributions of this study is the development of a 3D cardiac model using tissue engineering techniques to evaluate toxicological effects with higher physiological relevance to the adult human heart. While conventional 2D cultures lack the structural complexity of native tissues, 3D models better recapitulate physiological cell–cell interactions and spatial organization.[13,14] In this study, we engineered a cardiac tissue model by incorporating hPSC-derived cardiomyocytes into a collagen-based matrix, mimicking the structural and functional characteristics of native cardiac tissue. This platform enabled a comprehensive assessment of BPA toxicity over time, including morphological changes in mitochondria, contractile function, and electrophysiological properties.

Notably, mitochondrial changes were observed in the 3D cardiac model. In particular, structural changes in mitochondria and disruptions in contraction patterns were detected following exposure to 50 μM BPA. Given the central role of mitochondria in cellular metabolism processes, such as ATP production, calcium homeostasis, and redox balance, these findings suggest that BPA-induced mitochondrial dysfunction may affect the physiological development of cardiac tissue. As mitochondrial impairment is recognized as a major contributor to cardiovascular diseases, including heart failure and ischemic heart conditions, the ability to detect such changes *in vitro* is important.[39] These findings suggest that 3D cardiac tissue models may provide enhanced sensitivity for detecting structural and functional cardiotoxicity of environmental chemicals such as BPA.

In addition to mitochondrial dysfunction, our study confirmed that high BPA concentrations can induce significant electrophysiological disturbances in cardiomyocytes, further highlighting the multiple toxic effects of BPA on cardiac tissue. Acute exposure to 10 μM BPA led to the loss or irregular overshoot of spontaneous action potentials (Figure 5C and D). Consistent with these findings, Hyun et al. reported significant inhibition of ion channel activities, including Na^+ and Ca^2+ currents, decreased field potentials, and suppressed contractility in hPSC-CMs at BPA concentrations as low as 10 μM, indicating substantial electrophysiological toxicity.[8] However, steady-state BPA exposures at lower concentrations (0.05, 0.2, 0.5, and 1 μM) did not significantly alter the action potential properties. Cooper et al. also reported dose-dependent reductions in action potential duration and depolarization spike amplitude in hPSC-CMs exposed to increasing concentrations of BPA, with significant changes observed at concentrations of 10 μM and above.[40] Notably, they found that BPA exposure significantly decreased spontaneous electrical activity as measured by multi-electrode array analysis, indicating impairment of the intrinsic electrical rhythm of cardiomyocytes. This observation aligns well with our patch clamp findings, transient cessation of electrical activity (Figure 5C and D). Collectively, these findings show that high concentrations of BPA at 10 μM and above can disrupt the electrical rhythm and spontaneous activity of cardiomyocytes through ion channel inhibition and highlight electrophysiological profiling as a critical component of cardiotoxicity assessment.

Also, Ma et al. recently demonstrated that BPA has adverse effects on contractile function, even at low concentrations.[41] They reported that exposure to ⩽1 μM BPA significantly reduced contractile amplitude, induced sarcomeric disarray, and upregulated hypertrophic markers such as atrial natriuretic peptide and brain natriuretic peptide in hiPSC-derived cardiomyocytes and 3D cardiac organoids.[41] Although our study primarily focused on acute exposure to high BPA concentrations (10–50 μM), we also observed marked contractile dysfunction and mitochondrial deformation in 3D cardiac tissues under these conditions, revealed by beating analysis and TEM (Figure 6). These complementary findings suggest that both low-dose chronic exposure and high-dose acute exposure to BPA can disrupt cardiac contractile function through distinct but converging mechanisms, emphasizing the need for comprehensive dose- and model-specific toxicity evaluations.

In this study, we established an *in vitro* toxicity assessment platform to evaluate drug toxicity at different stages of cardiac development using a cardiomyocyte-specific reporter cell line. Notably, validation with a personalized hPSC line demonstrated reproducibility beyond cell line specificity and confirmed its potential applicability in personalized medicine. Furthermore, this approach may have promising applications in personalized drug development through the integration of diverse databases and AI-driven algorithms. Additionally, the tissue engineering-based 3D cardiac model facilitated the assessment of the physiological effects of cardiotoxic substances in an environment more closely resembling actual cardiac tissue. This integrative strategy complements conventional assays by enabling multimodal evaluation of developmental and functional cardiotoxicity. Overall, this approach is expected to evolve into a precise and reliable *in vitro* platform for new drug development and toxicological assessments in the future.

ORCID iDs

Soon-jung Park https://orcid.org/0000-0002-9384-6034
Seong Woo Choi https://orcid.org/0000-0002-7906-495X
Yun-Gwi Park https://orcid.org/0000-0002-7139-7637
Hye-Eun Shim https://orcid.org/0000-0002-3425-6333
Ji-hee Choi https://orcid.org/0009-0008-5689-6279
Kang Moo Huh https://orcid.org/0000-0002-2406-6659
Sung-Hwan Moon https://orcid.org/0000-0003-1858-0261
Sun-Woong Kang https://orcid.org/0000-0001-8862-2151

Ethical considerations

This study was conducted in accordance with the ethical guidelines of the Declaration of Helsinki and approved by the Public Institutional Review Board Designated by the Ministry of Health and Welfare of Republic of Korea (P01-202309-03-001).

Author contributions

S.-H.M and S.-W.K conceptualized and supervised the study. S.-J.P and S.W.C designed the experimental protocol. S.-J.P, S.W.C, Y-G.P, H.-E.S, J.C and K.M.H carried out all the experiments. S.-J.P, S.W.C, Y-G.P, and H.-E.S prepared the initial draft of the manuscript. All the authors reviewed and edited the paper.

Funding

The authors disclosed receipt of the following financial support for the research, authorship, and/or publication of this article: This research was supported by a grant (RS-2024-00331852) from the Ministry of Food and Drug Safety of Republic of

Korea, the Bio & Medical Technology Development Program (RS-2023-00220207) of the National Research Foundation of Korea (NRF), the Korean Fund for Regenerative Medicine (KFRM) grant (25A0203L1), and Korea Institute of Toxicology (2710008766).

Declaration of conflicting interests

The authors declared no potential conflicts of interest with respect to the research, authorship, and/or publication of this article.

Data availability statement

The data that support the findings of this study are available from the corresponding author upon reasonable request.

Supplemental material

Supplemental material for this article is available online.

References

1. Xing J, Zhang S, Zhang M, et al. A critical review of presence, removal and potential impacts of endocrine disruptors bisphenol A. *Comp Biochem Physiol C Toxicol Pharmacol* 2022; 254: 109275.
2. Costa HE and Cairrao E. Effect of bisphenol A on the neurological system: a review update. *Arch Toxicol* 2024; 98: 1–73. 20231019.
3. Bao W, Liu BY, Rong S, et al. Association between bisphenol A exposure and risk of all-cause and cause-specific mortality in US adults. *Jama Netw Open* 2020; 3. DOI: ARTN e2011620 10.1001/jamanetworkopen.2020.11620.
4. Lin MH, Lee CY, Chuang YS, et al. Exposure to bisphenol A associated with multiple health-related outcomes in humans: an umbrella review of systematic reviews with meta-analyses. *Environ Res* 2023; 237: 116900. 20230818.
5. Karmakar PC, Kang HG, Kim YH, et al. Bisphenol A affects on the functional properties and proteome of testicular germ cells and spermatogonial stem cells in vitro culture model. *Sci Rep* 2017; 7: 11858.
6. Wang K, Zhao Z and Ji W. Bisphenol A induces apoptosis, oxidative stress and inflammatory response in colon and liver of mice in a mitochondria-dependent manner. *Biomed Pharmacother* 2019; 117: 109182.
7. Cao Y, Hu D, Cai C, et al. Modeling early human cortical development and evaluating neurotoxicity with a forebrain organoid system. *Environ Pollut* 2023; 337: 122624.
8. Hyun SA, Lee CY, Ko MY, et al. Cardiac toxicity from bisphenol A exposure in human-induced pluripotent stem cell-derived cardiomyocytes. *Toxicol Appl Pharmacol* 2021; 428: 115696.
9. Ramakrishnan S and Wayne NL. Impact of bisphenol-A on early embryonic development and reproductive maturation. *Reprod Toxicol* 2008; 25: 177-183.
10. Ge Y, Ren F, Chen L, et al. Bisphenol A exposure induces apoptosis and impairs early embryonic development in Xenopus laevis. *Environ Pollut* 2021; 280: 116901.
11. Choi SW, Shin JS, Park SJ, et al. Antiviral activity and safety of remdesivir against SARS-CoV-2 infection in human pluripotent stem cell-derived cardiomyocytes. *Antiviral Res* 2020; 184. Article.
12. Mioulane M, Foldes G, Ali NN, et al. Development of high content imaging methods for cell death detection in human pluripotent stem cell-derived cardiomyocytes. *J Cardiovasc Transl Res* 2012; 5: 593–604.
13. Serras AS, Rodrigues JS, Cipriano M, et al. A critical perspective on 3D liver models for drug metabolism and toxicology studies. *Front Cell Dev Biol* 2021; 9: 626805.
14. Lelievre SA, Kwok T and Chittiboyina S. Architecture in 3D cell culture: an essential feature for in vitro toxicology. *Toxicol In Vitro* 2017; 45: 287–295.
15. Duval K, Grover H, Han LH, et al. Modeling physiological events in 2D vs. 3D cell culture. *Physiology (Bethesda)* 2017; 32: 266–277.
16. Liu C, Feng X, Li G, et al. Generating 3D human cardiac constructs from pluripotent stem cells. *EBioMedicine* 2022; 76: 103813.
17. Li J, Wiesinger A, Fokkert L, et al. Molecular and electrophysiological evaluation of human cardiomyocyte subtypes to facilitate generation of composite cardiac models. *J Tissue Eng* 2022; 13: 20417314221127908.
18. Hochman-Mendez C, Pereira de Campos DB, Pinto RS, et al. Tissue-engineered human embryonic stem cell-containing cardiac patches: evaluating recellularization of decellularized matrix. *J Tissue Eng* 2020; 11: 2041731420921482.
19. Lemoine MD, Mannhardt I, Breckwoldt K, et al. Human iPSC-derived cardiomyocytes cultured in 3D engineered heart tissue show physiological upstroke velocity and sodium current density. *Sci Rep* 2017; 7: 5464.
20. Sendra M, Cavia-Saiz M and Muniz P. Are the BPA analogues an alternative to classical BPA? Comparison between 2D and alternative 3D in vitro neuron model to assess cytotoxic and genotoxic effects. *Toxicology* 2024; 502: 153715.
21. Frtus A, Smolkova B, Uzhytchak M, et al. Mechanical regulation of mitochondrial dynamics and function in a 3D-engineered liver tumor microenvironment. *ACS Biomater Sci Eng* 2023; 9: 2408–2425.
22. Ma Y, He R, Deng B, et al. Advanced 3D bioprinted liver models with human-induced hepatocytes for personalized toxicity screening. *J Tissue Eng* 2025; 16: 20417314241313341.
23. Murkar RS, Wiese-Rischke C, Weigel T, et al. Developing human upper, lower, and deep lung airway models: combining different scaffolds and developing complex co-cultures. *J Tissue Eng* 2025; 16: 20417314241299076.
24. Joo H, Min S and Cho SW. Advanced lung organoids for respiratory system and pulmonary disease modeling. *J Tissue Eng* 2024; 15: 20417314241232502.
25. Nossa R, Costa J, Cacopardo L, et al. Breathing in vitro: designs and applications of engineered lung models. *J Tissue Eng* 2021; 12: 20417314211008696.
26. Creff J, Malaquin L and Besson A. In vitro models of intestinal epithelium: toward bioengineered systems. *J Tissue Eng* 2021; 12: 2041731420985202. 20210201.
27. Beauchamp P, Moritz W, Kelm JM, et al. Development and characterization of a scaffold-free 3D spheroid model of induced pluripotent stem cell-derived human cardiomyocytes. *Tissue Eng Part C Methods* 2015; 21: 852–861.
28. Park SJ, Kim H, Lee S, et al. Effect and application of cryopreserved three-dimensional microcardiac spheroids

in myocardial infarction therapy. *Clin Transl Med* 2022; 12: e721.
29. Hinton A, Jr., Katti P, Christensen TA, et al. A comprehensive approach to sample preparation for electron microscopy and the assessment of mitochondrial morphology in tissue and cultured cells. *Adv Biol (Weinh)* 2023; 7: e2200202.
30. Jin G, Floy ME, Simmons AD, et al. Spatial stem cell fate engineering via facile morphogen localization. *Adv Healthc Mater* 2021; 10: e2100995.
31. Park SJ, Kim RY, Park BW, et al. Dual stem cell therapy synergistically improves cardiac function and vascular regeneration following myocardial infarction. *Nat Commun* 2019; 10: 3123.
32. Park NK, Park YG, Choi JH, et al. Human induced pluripotent stem cell-cardiomyocytes for cardiotoxicity assessment: a comparative study of arrhythmiainducing drugs with multi-electrode array analysis. *Korean J Physiol Pharmacol* 2025; 29: 257–269.
33. Park YG, Park NK, Lee Y, et al. A machine learning platform for genotype-specific cardiotoxicity risk prediction using patient-derived iPSC-CMs. *J Adv Res* 2025. DOI: 10.1016/j.jare.2025.07.030
34. Escarda-Castro E, Herraez MP and Lombo M. Effects of bisphenol A exposure during cardiac cell differentiation. *Environ Pollut* 2021; 286: 117567.
35. Chen X, Xu B, Han X, et al. Effect of bisphenol A on pluripotency of mouse embryonic stem cells and differentiation capacity in mouse embryoid bodies. *Toxicol In Vitro* 2013; 27: 2249–2255.
36. Yin N, Yao X, Qin Z, et al. Assessment of Bisphenol A (BPA) neurotoxicity in vitro with mouse embryonic stem cells. *J Environ Sci (China)* 2015; 36: 181–187.
37. Posnack NG, Brooks D, Chandra A, et al. Physiological response of cardiac tissue to bisphenol A: alterations in ventricular pressure and contractility. *Am J Physiol Heart Circ Physiol* 2015; 309: H267–H275.
38. Posnack NG, Jaimes R, 3rd, Asfour H, et al. Bisphenol A exposure and cardiac electrical conduction in excised rat hearts. *Environ Health Perspect* 2014; 122: 384–390.
39. Peoples JN, Saraf A, Ghazal N, et al. Mitochondrial dysfunction and oxidative stress in heart disease. *Exp Mol Med* 2019; 51: 1–13.
40. Cooper BL, Salameh S and Posnack NG. Comparative cardiotoxicity assessment of bisphenol chemicals and estradiol using human induced pluripotent stem cell-derived cardiomyocytes. *Toxicol Sci* 2024; 198: 273–287.
41. Ma J, Ross S, Grube C, et al. Toxicity of low dose bisphenols in human iPSC-derived cardiomyocytes and human cardiac organoids – Impact on contractile function and hypertrophy. *Chemosphere* 2024; 353: 141567.